

A bearing fault feature extraction method based on cepstrum pre-whitening and a quantitative law of symplectic geometry mode decomposition

Chen Yiya¹ Jia Minping¹ Yan Xiaolan²

(¹ School of Mechanical Engineering, Southeast University, Nanjing 211189, China)

(² School of Mechatronics Engineering, Nanjing Forestry University, Nanjing 210037, China)

Abstract: In order to extract the fault feature of the bearing effectively and prevent the impact components caused by bearing damage being interfered with by discrete frequency components and background noise, a method of fault feature extraction based on cepstrum pre-whitening (CPW) and a quantitative law of symplectic geometry mode decomposition (SGMD) is proposed. First, CPW is performed on the original signal to enhance the impact feature of bearing fault and remove the periodic frequency components from complex vibration signals. The pre-whitening signal contains only background noise and non-stationary shock caused by damage. Secondly, a quantitative law that the number of effective eigenvalues of the Hamilton matrix is twice the number of frequency components in the signal during SGMD is found, and the quantitative law is verified by simulation and theoretical derivation. Finally, the trajectory matrix of the pre-whitening signal is constructed and SGMD is performed. According to the quantitative law, the corresponding feature vector is selected to reconstruct the signal. The Hilbert envelope spectrum analysis is performed to extract fault features. Simulation analysis and application examples prove that the proposed method can clearly extract the fault feature of bearings.

Key words: cepstrum pre-whitening; symplectic geometry mode decomposition; eigenvalue; quantitative law; feature extraction

DOI:10.3969/j.issn.1003-7985.2021.01.005

Rolling bearings play a key role in modern industry. The failure of the rolling bearing may lead to the failure of the whole mechanical system or even an accident^[1-2]. With the advantages of accurate positioning and convenient data collection, the vibration signal analysis is considered to be the most effective method in feature extraction and fault diagnosis^[3]. Vibration signals collected by vibration sensors mounted on bearing boxes are indi-

rect sources of information, which are usually interfered with by various noises. Fault feature signals are usually weak, which hinders the detection of bearing faults. Therefore, it is necessary to adopt effective signal processing methods to provide more obvious information for the fault diagnosis of rolling bearings^[4].

The failure modes of bearings mainly include pitting corrosion, spalling, abrasion, etc., among which spalling is the main fatigue damage type of ball bearings^[5]. When the bearing fails, the collision between the damaged part and the surface of other components will produce temporary impact components in the time domain. The bandwidth of the frequency domain is large, which covers the natural frequency of the bearing system and even the sensor, thus causing system resonance. Effective extraction of fault features can be obtained by envelope demodulation spectrum analysis, but the optimal resonance band should be selected, and the background noise in the mechanical system will seriously affect the accuracy of demodulation. In recent years, many advanced methods have been applied to bearing diagnosis. For example, Chen et al.^[6] proposed a fault diagnosis method based on the integration of resonance-based sparse signal decomposition (RSSD) and wavelet transform. Ding et al.^[7] proposed a dynamic structure adaptive sign method for predicting the life of slewing bearings under variable working conditions. Jiang et al.^[8] proposed a method based on minimum entropy deconvolution and envelop spectrum analysis. However, the above method requires a huge amount of calculation, and the effect of background noise on fault feature extraction is not considered.

In 2011, Sawalhi and Randall^[9] proposed a signal pre-whitening method based on the cepstrum editing procedure (CEP). By editing the cepstrum value of the vibration signal, the corresponding cepstrum value in the real cepstrum is set to be zero to obtain the pre-whitening signal. The advantage of this method is that there is no need to select the resonance frequency band, and the envelope analysis can improve the bearing fault diagnosis effect; however, there is the disadvantage of increased noise interference^[10]. SGMD is a new nonlinear dynamic decomposition method based on the symplectic geometry similarity transformation proposed by Pan et al.^[11]. Existing decomposition algorithms include wavelet transform^[12], ensemble empirical mode decomposition (EEMD)^[13],

Received 2020-08-10, **Revised** 2020-11-12.

Biographies: Chen Yiya (1995—), female, graduate; Jia Minping (corresponding author), male, doctor, professor, mpjia@seu.edu.cn.

Foundation item: The National Natural Science Foundation of China (No. 52075095).

Citation: Chen Yiya, Jia Minping, Yan Xiaolan. A bearing fault feature extraction method based on cepstrum pre-whitening and a quantitative law of symplectic geometry mode decomposition. [J]. Journal of Southeast University (English Edition), 2021, 37(1): 33–41. DOI:10.3969/j.issn.1003-7985.2021.01.005.

local feature-scale decomposition (LCD)^[14], and singular spectrum analysis (SSA)^[15] etc. These methods have some defects for the signal analysis of the nonlinear system. When the signal is more complex, especially with noise, LCD and SSA will force the signal to decompose into several incomplete components. In addition, wavelet transform and EEMD require user-defined parameters and are very sensitive to parameters^[11]. SGMD can effectively reconstruct the signal and eliminate noise without any user-defined parameters.

However, SGMD also has certain disadvantages. First, SGMD directly constructs the trajectory matrix through the original time series. Under background noise, weak fault features may be drowned in the global time series. Secondly, SGMD reconstructs the final symplectic geometry mode component by calculating the frequency similarity and component correlation of the initial components, which requires a large amount of computation and lacks a theoretical basis. Based on these two shortcomings, this paper combines the signal pre-whitening method based on CEP and the quantitative law of SGMD. Firstly, the original fault signal is preprocessed by CPW to remove the discrete frequency component in the signal and eliminate its interference in the unsteady shock component caused by bearing damage. Secondly, SGMD is performed, and the bearing fault signal was reconstructed according to the quantitative law of eigenvalues found in the SGMD. Finally, the reconstructed signal was analyzed by the Hilbert envelope spectrum to realize the effective extraction of bearing fault features. Moreover, simulations and experiments are carried out to verify the effectiveness of the proposed method.

1 Cepstrum Pre-Whitening

CPW means to set all the values to be zero in the real cepstrum domain. It removes discrete frequency components such as harmonics and sidebands in the signal spectrum to obtain the best smooth distribution of discrete frequency components in the signal spectrum. The pre-whitening signal contains only non-stationary impact components caused by white noise and bearing damage. Signal pre-whitening process based on cepstrum editing enhances the vibration shock components of bearing fault signals. The schematic diagram of the CPW of vibration signal is shown in Fig. 1.

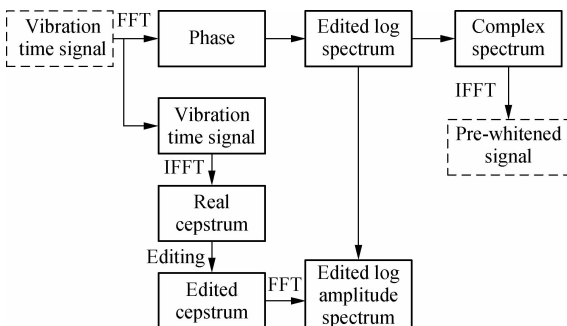


Fig. 1 Schematic diagram of the cepstrum pre-whitening procedure

The signal pre-whitening process essentially removes all discrete frequency components and resonance effects in the original vibration signal. It turns the entire spectrum of the pre-whitened signal into a resonance frequency band. Therefore, there is no need to determine the optimal resonance frequency band. Pre-whitened signals can be directly enveloped. However, it does not remove much white noise in the weak bearing failure and the results of envelope demodulation are not obvious.

2 Simulation Analysis and Theoretical Derivation of SGMD's Quantitative Law

SGMD reconstructs the final symplectic geometric modal component by calculating the frequency similarity and component correlation of the initial symplectic geometry components (SGCs), which is computationally intensive and lacks a theoretical basis, and it easily attracts noise. The initial SGCs are positive. It is the eigenvector corresponding to the eigenvalue of the Hamilton matrix during the decomposition process. Therefore, this paper explores and finds the quantitative relationship between its eigenvalue and the number of frequencies in the original signal, and theoretically derives the quantitative law to better understand the physical meaning of the initial SGCs.

2.1 Symplectic geometry mode decomposition

2.1.1 Phase-space reconstruction

The original time series can be expressed as $s = x_1, x_2, \dots, x_n$, where n is the length of the time series, and X is obtained by the phase-space reconstruction of the raw time series:

$$X = \begin{bmatrix} x_1 & x_{1+\tau} & \cdots & x_{1+(d-1)\tau} \\ x_2 & x_{2+\tau} & \cdots & x_{2+(d-1)\tau} \\ \vdots & \vdots & \cdots & \vdots \\ x_m & x_{m+\tau} & \cdots & x_{m+(d-1)\tau} \end{bmatrix} \quad (1)$$

where d is the embedding dimension, and τ is the delay time, and $m = n - (d-1)\tau$. By selecting the appropriate embedding dimension d and the delay time τ , the corresponding reconstruction matrix X can be obtained. In this paper, the PSD is used to ascertain the embedding dimension. When the normalized frequency is less than 0.001, $k = n/3$, otherwise $k = 1.2 \times (f_{\max}/f_s)$, where f_{\max} is the frequency of the maximum peak in the PSD and f_s is the sampling frequency.

2.1.2 Symplectic geometry similarity transformation

The reconstruction matrix X can construct the Hamilton matrix $M = \begin{bmatrix} B & O \\ O & -B^T \end{bmatrix}$, where $B = X^T X$. Then, we can obtain a symplectic orthogonal matrix Q :

$$Q^T M Q = \begin{bmatrix} H & R \\ O & H^T \end{bmatrix} \quad (2)$$

In the process of symplectic transformation, the structural features of the Hamilton matrix are preserved, so the transformed matrix is still a Hamilton matrix. H is the upper tri-

angular matrix. We calculate the eigenvalues $\sqrt{\lambda(\mathbf{H})}$ of the matrix \mathbf{H} . $\lambda(\mathbf{M}) = \lambda(\mathbf{H})$ and $\lambda(\mathbf{B}) = \sqrt{\lambda(\mathbf{M})} = \sqrt{\lambda(\mathbf{H})}$ can be obtained by the properties of the Hamilton matrix. d is the number of eigenvalues, and the eigenvalues λ_i of matrix \mathbf{H} can be expressed as $\lambda_1, \lambda_2, \dots, \lambda_d$. According to the properties of the Hamilton matrix, the eigenvalues of matrix \mathbf{B} are calculated as follows:

$$\sigma_i = \sqrt{\lambda_i} \quad i = 1, 2, \dots, d \quad (3)$$

The eigenvalues of matrix \mathbf{B} are arranged in a descending order as

$$\sigma_1 > \sigma_2 > \dots > \sigma_d \quad (4)$$

\mathbf{Q}_i is the eigenvector corresponding to the eigenvalue σ_i of matrix \mathbf{B} . Let $\mathbf{S}_i = \mathbf{Q}_i^T \mathbf{X}^T$, $\mathbf{Z}_i = \mathbf{Q}_i \mathbf{S}_i$ ($i = 1, 2, \dots, d$), and a new reconstruction matrix \mathbf{Z}_i can be obtained. Then, the reconstructed phase-space matrix can be expressed as

$$\mathbf{Z} = \mathbf{Z}_1 + \mathbf{Z}_2 + \dots + \mathbf{Z}_d \quad (5)$$

2.1.3 Diagonal averaging

Let $\mathbf{Z}_{m \times d} = (z_{ij})_{m \times d}$ where $1 \leq i \leq m, 1 \leq j \leq d$. $d^* = \min(m, d)$, $m^* = \max(m, d)$ and $n = m + (d - 1)\tau$. Meanwhile, $y_{ij}^* = z_{ij}$, if $m < d$, otherwise, $y_{ij}^* = z_{ji}$.

$$y_i = \begin{cases} \frac{1}{t} \sum_{d=1}^t y_{q,t-q+1}^* & 1 \leq t \leq d^* \\ \frac{1}{d^*} \sum_{q=1}^{d^*} y_{q,t-q+1}^* & d^* \leq t \leq m^* \\ \frac{1}{n-t+1} \sum_{q=t-m^*+1}^{n-m^*+1} y_{q,t-q+1}^* & m^* \leq t \leq n \end{cases} \quad (6)$$

By Eq. (6), we can determine $Y_i(y_1, y_2, \dots, y_n)$, and a set of series Y_i with one-dimensional length n corresponding to matrix \mathbf{Z}_i is obtained. The initial SGCs obtained from the diagonal averaging can be expressed as

$$\mathbf{Y} = \mathbf{Y}_1 + \mathbf{Y}_2 + \dots + \mathbf{Y}_d \quad (7)$$

2.1.4 Components reorganization

First, similar components with high similarity are summed to obtain the first component SGC₁. Then, the reconstructed components of SGC₁ are removed from matrix \mathbf{Y} , and the remaining matrix can be expressed as \mathbf{G}_1 . Finally, the remaining signal g_1 is obtained by summing the residual signal, and the normalized mean square error E between the residual and the original signal is then calculated as

$$E^h = \frac{\sum_{e=1}^n g^h(e)}{\sum_{e=1}^n x(e)} \quad (8)$$

where h is the number of iterations. When the normalized mean squared error is less than the given threshold 1%, the whole decomposition process will end. Otherwise, the residual matrix is used as the iterative original matrix to repeat the above iterative process until the iterative stopping condition is satisfied, and the final decomposi-

tion result is obtained as

$$x(n) = \sum_{h=1}^N \text{SGC}^h(n) + g^{(N+1)}(n) \quad (9)$$

where N is the number of component series identified.

2.2 Simulation analysis of the quantitative law in SGMD algorithm

During the process of SGMD, it is found that there is an important relationship between symplectic geometric spectrum σ_i of matrix \mathbf{B} and the number of signal frequencies. The smaller value of σ_i (close to zero) is regarded as the noise component, and the larger value of σ_i (not close to zero) is the effective eigenvalue of matrix \mathbf{B} , which is denoted as α_i .

By the method of repeated experiments, the number of frequencies in the signal gradually increases from 1 to 8, and each signal adds a frequency component to the previous signal. Then, the trajectory matrix with the same dimension is constructed for SGMD. The changes in the number of α_i are observed and analyzed during the process. The signal expression is

$$\left. \begin{aligned} y_1(t) &= 3\sin(t + 0.66) \\ y_2(t) &= y_1(t) + 5.6\sin(3t + 0.86) \\ y_3(t) &= y_2(t) + 12\sin(10t + 0.98) \\ y_4(t) &= y_3(t) + 15\sin(8t + 1.28) \\ y_5(t) &= y_4(t) + 18\sin(24t + 1.58) \\ y_6(t) &= y_5(t) + 24\sin(32t + 2.58) \\ y_7(t) &= y_6(t) + 30\sin(39t + 0.58) \\ y_8(t) &= y_7(t) + 38\sin(52t + 0.98) \end{aligned} \right\} \quad (10)$$

In order to verify the influence of noise on the results, each signal in Eq. (10) is added with the noise of -5 and -10 dB. The sampling frequency of each signal is 1 024 Hz, and 1 024 points are collected in $[0, 2\pi]$. The dimension of the constructed trajectory matrix is 522×523 . The symplectic geometry of matrix \mathbf{B} in SGMD is calculated, and the results are shown in Fig. 2.

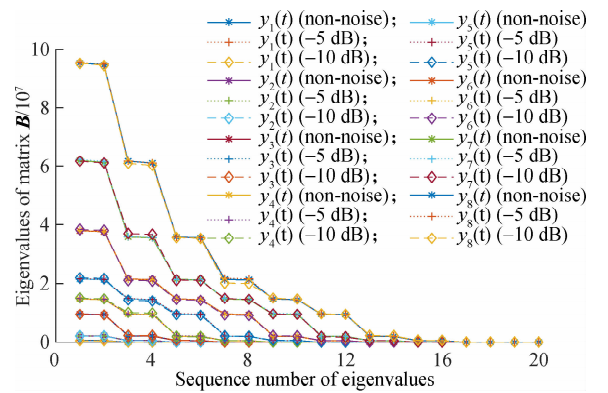


Fig. 2 Symplectic spectrum of matrix \mathbf{B}

It can be seen from Fig. 2 that the number of effective eigenvalues in the symplectic geometric spectrum of frequency component matrix \mathbf{B} is always increased by only two for every increase of a frequency in the signal. In the

symplectic geometry spectrum of the newly added signal, except for the two newly added eigenvalues, the rest of the eigenvalues are almost the same as the eigenvalue of the previous signal, and the two newly added eigenvalues are almost equal. If other frequencies and amplitudes are used for decomposition, the same result will be obtained; that is, one frequency component always corresponds to two effective eigenvalues, and is independent of frequency, amplitude and signal-noise ratio.

In summary, the number of α_i is determined by the number of frequencies in the signal and is independent of the frequency size, amplitude and phase. As long as the dimension of the trajectory matrix constructed by the signal is greater than twice the number of frequencies in the signal, each frequency component will correspond to two α_i . Since the corresponding eigenvector of α_i is the initial SGC, every two

initial SGCs correspond to a frequency component.

2.3 Theoretical derivation of the quantitative law in SGMD algorithm

In order to verify the correctness of the quantitative law in Section 2.2, this section makes a theoretical derivation of the double quantity relationship between α_i and the number of signal frequencies in the symplectic geometry mode decomposition process. There is a continuous deterministic signal $y(t)$ in the time domain, including i frequency components, which is expressed as

$$y(t) = \sum_{i=1}^I A_i \sin(\omega_i t + \varphi_i) \quad (11)$$

Sampling Eq. (11) at equal time intervals, the constructed trajectory matrix is

$$X_i = \begin{bmatrix} a_i \sin(\omega_i T_s \cdot 0 + \varphi_i) & a_i \sin(\omega_i T_s \cdot 1 + \varphi_i) & \cdots & a_i \sin(\omega_i T_s \cdot (n-1) + \varphi_i) \\ a_i \sin(\omega_i T_s \cdot 1 + \varphi_i) & a_i \sin(\omega_i T_s \cdot 2 + \varphi_i) & \cdots & a_i \sin(\omega_i T_s \cdot n + \varphi_i) \\ \vdots & \vdots & \ddots & \vdots \\ a_i \sin(\omega_i T_s \cdot (m-1) + \varphi_i) & a_i \sin(\omega_i T_s \cdot m + \varphi_i) & \cdots & a_i \sin(\omega_i T_s \cdot (N-1) + \varphi_i) \end{bmatrix} \quad (12)$$

According to the trigonometric function relation, we can obtain

$$\sin(\omega_i t + \varphi_i) = a_i \sin(\omega_i t) + b_i \cos(\omega_i t) \quad (13)$$

where $\varphi_i = \arctan\left(\frac{b_i}{a_i}\right)$, $\sqrt{a_i^2 + b_i^2} = 1$, $a_i \neq 0$. Substituting Eq. (13) into Eq. (12), we can obtain

$$X_i = A_i \left\{ a_i \begin{bmatrix} \sin(\omega_i T_s \cdot 0) & \sin(\omega_i T_s \cdot 1) & \cdots & \sin(\omega_i T_s \cdot (n-1)) \\ \sin(\omega_i T_s \cdot 1) & \sin(\omega_i T_s \cdot 2) & \cdots & \sin(\omega_i T_s \cdot n) \\ \vdots & \vdots & \ddots & \vdots \\ \sin(\omega_i T_s \cdot (m-1)) & \sin(\omega_i T_s \cdot m) & \cdots & \sin(\omega_i T_s \cdot (N-1)) \end{bmatrix} + b_i \begin{bmatrix} \cos(\omega_i T_s \cdot 0) & \cos(\omega_i T_s \cdot 1) & \cdots & \cos(\omega_i T_s \cdot (n-1)) \\ \cos(\omega_i T_s \cdot 1) & \cos(\omega_i T_s \cdot 2) & \cdots & \cos(\omega_i T_s \cdot n) \\ \vdots & \vdots & \ddots & \vdots \\ \cos(\omega_i T_s \cdot (m-1)) & \cos(\omega_i T_s \cdot m) & \cdots & \cos(\omega_i T_s \cdot (N-1)) \end{bmatrix} \right\} \quad (14)$$

By the Euler formula $e^{j\omega T_s} = \cos\omega T_s + j\sin\omega T_s$, we can obtain

$$\sin(\omega_i T_s) = \frac{e^{j\omega_i T_s} - e^{-j\omega_i T_s}}{2j}, \quad \cos(\omega_i T_s) = \frac{e^{j\omega_i T_s} + e^{-j\omega_i T_s}}{2} \quad (15)$$

Substituting Eq. (15) into Eq. (14) and by simplification, we can obtain

$$X_i = A_i \left\{ \left(\frac{a_i}{2j} + \frac{b_i}{2} \right) \begin{bmatrix} e^{j\omega_i T_s \cdot 0} & e^{j\omega_i T_s \cdot 1} & \cdots & e^{j\omega_i T_s \cdot (n-1)} \\ e^{j\omega_i T_s \cdot 1} & e^{j\omega_i T_s \cdot 2} & \cdots & e^{j\omega_i T_s \cdot n} \\ \vdots & \vdots & \ddots & \vdots \\ e^{j\omega_i T_s \cdot (m-1)} & e^{j\omega_i T_s \cdot m} & \cdots & e^{j\omega_i T_s \cdot (N-1)} \end{bmatrix} + \left(\frac{a_i}{2j} - \frac{b_i}{2} \right) \begin{bmatrix} e^{-j\omega_i T_s \cdot 0} & e^{-j\omega_i T_s \cdot 1} & \cdots & e^{-j\omega_i T_s \cdot (n-1)} \\ e^{-j\omega_i T_s \cdot 1} & e^{-j\omega_i T_s \cdot 2} & \cdots & e^{-j\omega_i T_s \cdot n} \\ \vdots & \vdots & \ddots & \vdots \\ e^{-j\omega_i T_s \cdot (m-1)} & e^{-j\omega_i T_s \cdot m} & \cdots & e^{-j\omega_i T_s \cdot (N-1)} \end{bmatrix} \right\} \quad (16)$$

X_i can be rewritten as the sum of two matrices as

$$X_i = A_i \left(\left(\frac{a_i}{2j} + \frac{b_i}{2} \right) X_{i1} + \left(\frac{a_i}{2j} - \frac{b_i}{2} \right) X_{i2} \right) \quad (17)$$

$$X_{i2} = \begin{bmatrix} e^{-j\omega_i T_s \cdot 0} & e^{-j\omega_i T_s \cdot 1} & \cdots & e^{-j\omega_i T_s \cdot (n-1)} \\ e^{-j\omega_i T_s \cdot 1} & e^{-j\omega_i T_s \cdot 2} & \cdots & e^{-j\omega_i T_s \cdot n} \\ \vdots & \vdots & \ddots & \vdots \\ e^{-j\omega_i T_s \cdot (m-1)} & e^{-j\omega_i T_s \cdot m} & \cdots & e^{-j\omega_i T_s \cdot (N-1)} \end{bmatrix}$$

where

$$X_{i1} = \begin{bmatrix} e^{j\omega_i T_s \cdot 0} & e^{j\omega_i T_s \cdot 1} & \cdots & e^{j\omega_i T_s \cdot (n-1)} \\ e^{j\omega_i T_s \cdot 1} & e^{j\omega_i T_s \cdot 2} & \cdots & e^{j\omega_i T_s \cdot n} \\ \vdots & \vdots & \ddots & \vdots \\ e^{j\omega_i T_s \cdot (m-1)} & e^{j\omega_i T_s \cdot m} & \cdots & e^{j\omega_i T_s \cdot (N-1)} \end{bmatrix}$$

X is the sum of the trajectory matrix X_i constructed by a single frequency component:

$$X = \sum_{i=1}^I X_i \quad (18)$$

From Eq. (17) and Eq. (18), the total trajectory matrix containing I frequency component signals can be obtained as

$$\mathbf{X} = \sum_{i=1}^I \mathbf{X}_i = \sum_{i=1}^I \mathbf{A}_i \left(\left(\frac{a_i}{2j} + \frac{b_i}{2} \right) \mathbf{X}_{i1} + \left(\frac{a_i}{2j} - \frac{b_i}{2} \right) \mathbf{X}_{i2} \right) \quad (19)$$

It can be seen from Eq. (19) that the total trajectory matrix \mathbf{X} is obtained by summing up I trajectory matrix \mathbf{X}_i , and it can be proved that the rank of the trajectory matrix \mathbf{X}_i is 2 and is only related to frequency. Since $\omega_1 \neq \omega_2 \neq \omega_3 \neq \dots \neq \omega_I$, the trajectory matrix \mathbf{X}_i formed by each frequency signal is linearly independent. Therefore, when the original signal contains I frequency components and the total matrix \mathbf{X} satisfies $\min(m, n) \geq 2I$, the rank of the total matrix \mathbf{X} is $2I$. In the SGMD process, since the matrix $\mathbf{B} = \mathbf{X}^T \mathbf{X}$, $r(\mathbf{B}) = r(\mathbf{X}^T \mathbf{X}) = r(\mathbf{X}) = 2I$ can be obtained. The number of non-zero eigenvalues of a matrix is equal to the rank of the matrix, so the number of effective eigenvalues of matrix \mathbf{B} obtained after SGMD should also be $2I$, and is independent of amplitude and phase.

According to the above simulation and theoretical derivation, it can be seen that the feature frequency component of the vibration signal is included in the feature value sequence spectrum. In the following, the SGMD's quantitative law will be further applied to the extraction of feature frequencies of bearing fault simulation signals and experimental vibration signals.

3 Procedures of the Proposed Method for Fault

In this paper, a bearing fault feature extraction method based on CPW and SGMD quantitative law is proposed. CPW can remove the discrete frequency components in the signal, so that the entire frequency spectrum of the pre-whitening signal becomes a resonance frequency band. There is no need to determine the optimal resonance frequency band, and the pre-whitening signal can be directly enveloped and analyzed. The double relationship between the number of effective eigenvalues of the Hamilton matrix and the number of signal frequencies during the SGMD indicates that every two initial SGCs correspond to a frequency component in the signal, so that the corresponding initial SGCs can be combined to extract feature frequencies and reduce the amount of calculation. Moreover, the detailed process of the proposed method is illustrated as follows:

1) First, CPW is used to preprocess the bearing fault signals and remove the discrete frequency components so as to eliminate its interference in the unsteady impact components caused by bearing damage.

2) Subsequently, the envelope spectrum analysis is performed on the signal after CPW, and preliminary feature extraction is performed.

3) Construct the trajectory matrix for the pre-processed signal, conduct SGMD and obtain the initial SGCs.

4) Finally, according to the SGMD's quantitative law, select the eigenvalues corresponding to the corresponding fault feature frequency components in the envelope spectrum, and reconstruct the eigenvectors (initial SGCs) corresponding to these eigenvalues. The signal was analyzed by the Hilbert envelope spectrum to extract the feature frequency of the fault.

4 Simulation Analysis

To validate the excellent effectiveness of the proposed algorithm in extracting feature frequencies, this section will employ an emulation of the simple rolling bearing model. Consequently, the simulated vibration signal of a bearing with partial failure is established as follows^[16]:

$$\left. \begin{aligned} x(t) &= x_1(t) + x_2(t) + i(t) \quad t \in (0, 1) \\ x_1(t) &= \sin(2\pi f_1 t) + \sin(2\pi f_2 t) + \sin(2\pi f_3 t) + \sin(2\pi f_4 t) \\ i(t) &= 1.2(\exp(-100t_1))\sin(600\pi t) \quad t_1 = \text{mod}(t, 1/f_0) \end{aligned} \right\} \quad (20)$$

The simulation signal $x(t)$ is composed of $x_1(t)$, $x_2(t)$ and $i(t)$. The sinusoidal signal frequency components f_1, f_2, f_3 , and f_4 are 18, 56, 100 and 200 Hz, respectively, and are used to simulate the number of interference sources when bearing failures occur. Signal $x_2(t)$ is applied to simulate the white noise, which can be generated in Matlab using the function `awgn`. Signal $i(t)$ is employed to imitate the periodic impulses; the amplitude is 1.2; the natural frequency is 300 Hz; and the pulse feature frequency is $f_0 = 15$ Hz. Here, the sampling length is $N = 10\,240$, and the sampling frequency is 10 240 Hz. The waveform, FFT spectrum and envelope spectrum of the simulation signal $x(t)$ are depicted in Fig. 3.

It can be seen from Fig. 3 that the transient impact features of the signal $x(t)$ are disturbed by the background

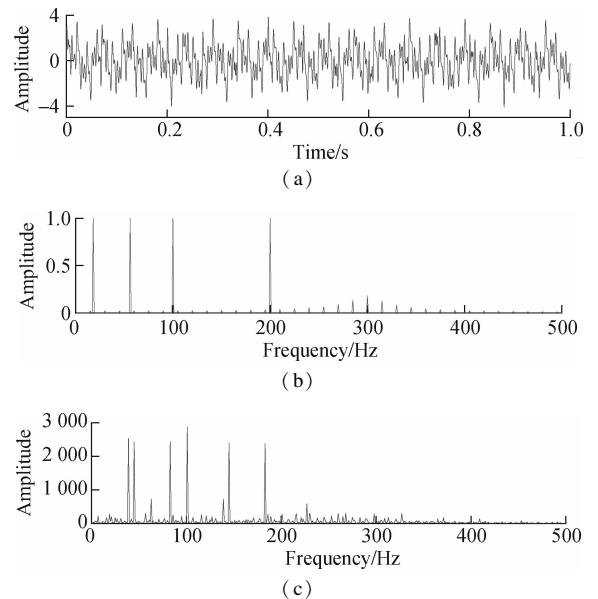


Fig. 3 Vibration signal waveform and spectrum. (a) Waveform; (b) FFT spectrum; (c) Envelope spectrum for simulation signal $x(t)$

noise and cannot be clearly identified. Its spectrum and envelope spectrum have no prominent spectral lines at f_o , and the extraction effect is not good. Therefore, the method of this paper is used to analyze the simulation signal, as shown in Fig. 4. Fig. 4(a) and Fig. 4(b) are the time-domain waveform and envelope spectrum of the CPW signal, respectively. The bearing fault feature frequency f_o and its harmonics can be seen from the envelope spectrum in Fig. 4(b).

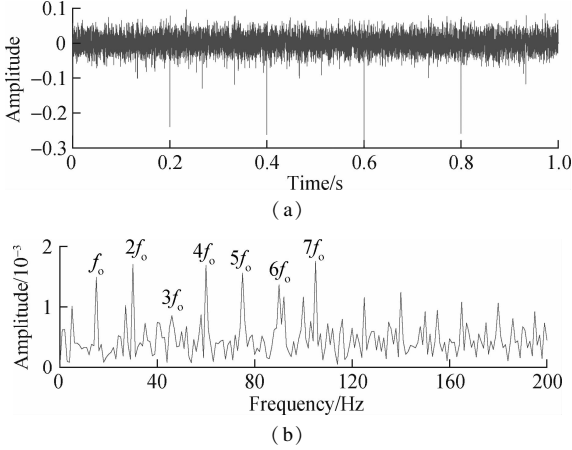


Fig. 4 Pre-whitening signal waveform and spectrum. (a) Time-domain waveform; (b) Envelope spectrum of the CEP pre-whitening signal

In order to further purify the fault features of the bearing and verify the quantitative law in SGMD, the trajectory matrix of the above pre-whitening signal is constructed, and then SGMD is carried out and the symplectic geometry spectrum of matrix B is solved, as shown in Fig. 5. It can be seen from the envelope spectrum of Fig. 4(b) that the magnitudes of the feature frequencies of the bearing faults are arranged from large to small as follows: $2f_o$, $4f_o$, $7f_o$, $5f_o$, $6f_o$ and $3f_o$, respectively. The value spectrum ranks first, second, third, fourth, and fifth, and the amplitude of $3f_o$ is relatively small, almost drowned in the envelope spectrum. The above research shows that in the process of SGMD, the number of effective eigenvalues of matrix B is twice that of the frequencies in the signal. Therefore, the eigenvalues corresponding to the top 5 frequencies of amplitude are the first 10 eigenvalues in matrix B symplectic spectrum. The eigenvector Q_i ($i = 1, 2, \dots, 10$) corresponding to these 10 eigenvalues is selected for reconstruction, and then the signal is recovered through diagonal averaging. The envelope spectrum is obtained as shown in Fig. 6.

It can be seen from the envelope spectrum that the fre-

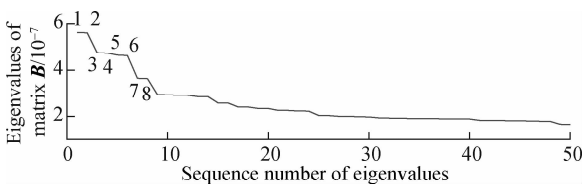


Fig. 5 Symplectic geometry spectrum of matrix B in SGMD after pre-whitening signal

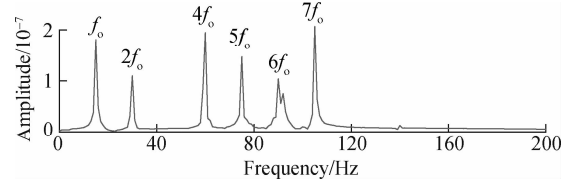


Fig. 6 Envelope spectrum of SGMD reconstructed signal

quency component of the reconstructed signal is only the fault frequency component of the bearing, and their amplitude is basically the same as the amplitude spectrum after pre-whitening. There are some differences due to the influence of noise in Fig. 4(b). It is inevitable that it can be said that the fault feature frequency and its multiplier can be basically completely extracted via the SGMD's quantitative law.

The feature frequency of the shock and its multiples in Fig. 6 are clearly extracted. Compared to the direct envelope spectrum analysis of the pre-whitening signal in Fig. 4, the SGMD reconstructed spectrum diagram clearly shows the feature frequency of the bearing failure. It shows that the method in this paper can effectively extract the features of weak bearings under the influence of background noise and interference frequency, and has good noise reduction and separation performance for vibration signals.

For comparison, the fault feature extraction method of the wavelet-SVD difference spectrum^[17] is introduced to process the above-mentioned simulation signals. First, using the "db5" wavelet coefficient, wavelet decomposition of the signal is performed on 5 scales, and then SVD is performed on the detailed signals of each scale (d1, d2, d3, d4, and d5) to obtain the singular value difference spectrum in Fig. 7. Each detail signal is reconstructed according to the singular value difference spectrum, and the spectrum of the reconstructed signal is shown in Fig. 8. The main frequency component in the frequency spectrum of the detailed signal d3 has an edge frequency. It is an amplitude-modulated signal. It is demodulated by the Hilbert transform. The envelope spectrum is shown in Fig. 9, and the fault feature frequency f_o and its harmonics can be obtained. This is consistent with the fault feature frequency extracted by the method proposed in this paper, which further verifies the accuracy of the method. However, the selection of small and medium wave coefficients and the determination of the decomposition scale in this method have a great impact on the accuracy of the analysis results. Moreover, SVD is required for every detail signal after wavelet decomposition, which requires a huge amount of computation and much time. The method proposed in this paper only needs to construct a trajectory matrix for pre-whitening signals after CPW, and perform SGMD, which requires less calculation and greatly improves the calculation efficiency. Moreover, it is found through comparison that the method used in this paper to extract bearing fault features is more obvious.

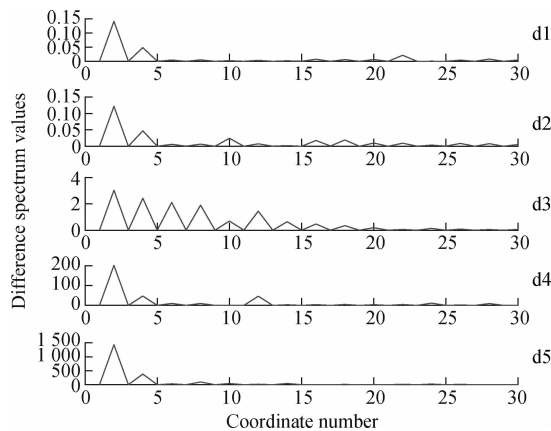


Fig. 7 Singular value difference spectrum of wavelet detail signals

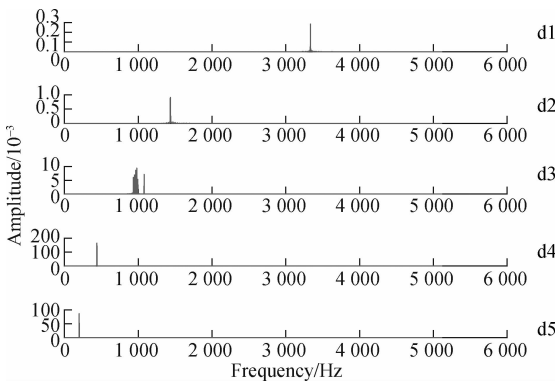


Fig. 8 Envelope spectrum of wavelet detail signal based on SVD reconstruction

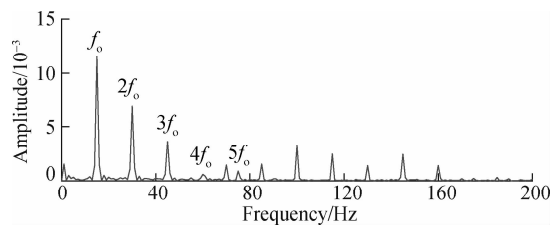


Fig. 9 Envelope spectrum of wavelet detail signal d3

5 Experimental Validation

In this section, the accelerated bearing life tester (ABLT-1A), provided by the Hangzhou Bearing Test and Research Center, is adopted to further confirm the performance of the proposed method. The test rig is shown in Fig. 10, which mainly consists of the loading system, lubrication system, transmission system, electrical control system, and computer monitoring system. The detailed parameters of the analyzed bearing are listed in Tab. 1. The rotation speed is 1 050 r/min. The sampling frequency and length are set to be 10 240 Hz and 10 240, respectively. Moreover, the feature frequency of the bearing fault is listed in Tab. 2.

Next, the raw vibration signal of the rolling bearing with the inner and outer fault is selected for analysis, as shown in Fig. 11 (a). Its FFT spectrum and envelope spectrum are described in Figs. 11(b) and (c), respec-

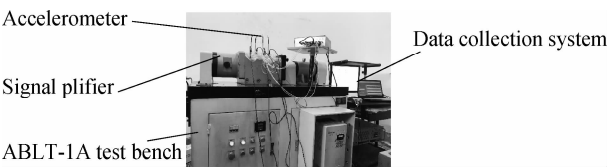


Fig. 10 Experimental device

Tab. 1 Parameters of the deep groove ball bearing

Bearing type	Roller diameter/ mm	Pitch diameter/ mm	Number of rollers	Contact angle/ (°)
HRB 6205	7.5	38.5	9	0

Tab. 2 Rolling bearing theoretical fault feature frequency

Type of failure	Inner-race f_i	Outer-race f_o	Rollers f_b	Cage f_c
Fault feature frequency/Hz	61	95	43	86

tively. It can be seen that the transient impact features of the signal are overwhelmed by background noise and interference signals, and the impact phenomenon is not obvious. In the envelope spectrum, there are no prominent spectral line peaks at the feature frequencies f_o and f_i . The prominent spectral line frequency and the fault feature frequency do not correspond with each other, and the fault feature extraction effect is not good.

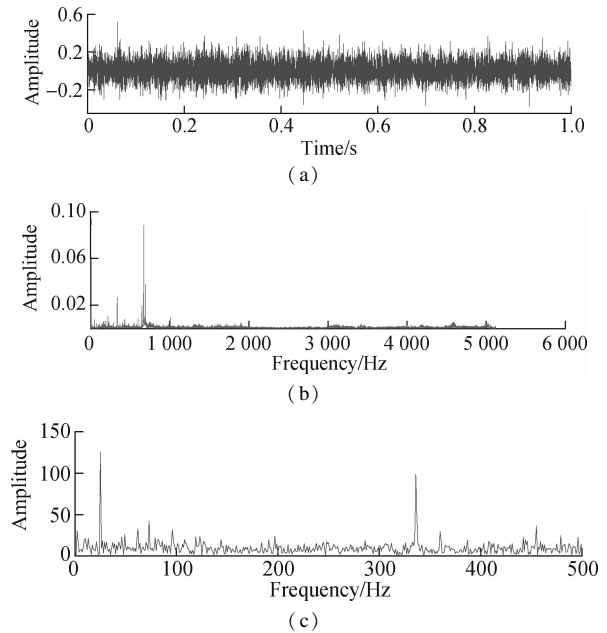


Fig. 11 Vibration signal waveform and spectrum and envelope spectrum of bearing fault. (a) Waveform; (b) Spectrum; (c) Envelope spectrum

The proposed method is therefore exploited to analyze the experimental signal and detect the rolling bearing fault. Figs. 12(a) and (b) show the time-domain waveform and envelope spectrum of the pre-whitening signal of the faulty bearing, respectively. From the envelope spectrum of Fig. 12(b), the fault feature frequencies of bearing inner-race f_i and outer-race fault feature frequency f_o can be clearly seen.

The trajectory matrix consists of the pre-whitening signal, SGMD is performed and the symplectic geometry spectrum of matrix B is solved(as shown in Fig. 13). It can be

seen from the envelope spectrum of Fig. 12(b) that the amplitudes of the spectral lines, where the feature frequencies of the bearing faults are arranged from large to small, are f_o , $2f_o$, f_i , $3f_o$, and $2f_i$, and the amplitudes of these frequency components ranks, respectively, the first, the second, the third, the fourth, and the sixth are in the amplitude spectrum. From the above studies in this paper, we can find that the eigenvalues corresponding to these five frequencies are the first 8 eigenvalues and the 11th to 12th eigenvalues in matrix B symplectic geometry spectrum. The feature vectors corresponding to these feature values are selected for reconstruction. Then, the signal is recovered through diagonal averaging, and its envelope spectrum is obtained as shown in Fig. 14.

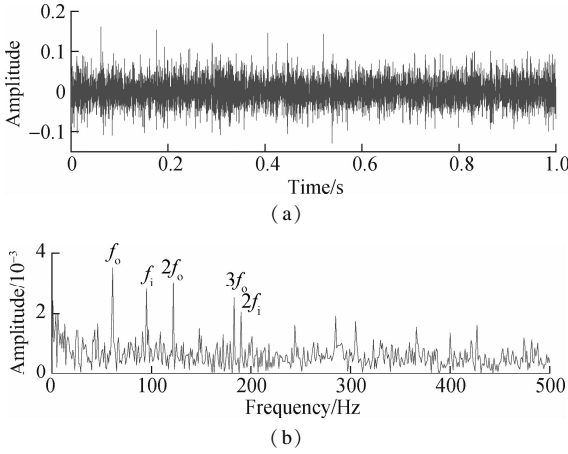


Fig. 12 Pre-whitening signal and envelope spectrum of bearing fault vibration. (a) Pre-whitening signal; (b) Envelope spectrum

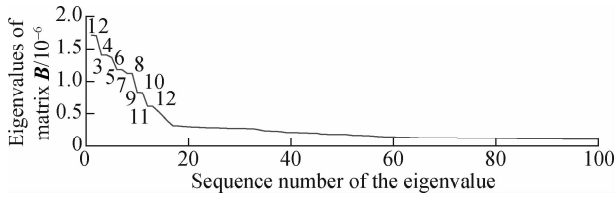


Fig. 13 Symplectic geometry spectrum of matrix B in SGMD

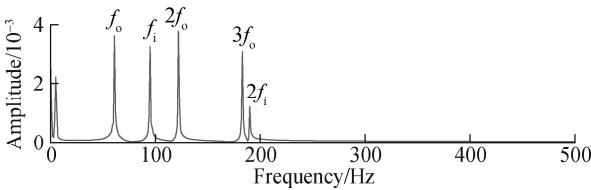


Fig. 14 Envelope spectrum of SGMD reconstructed signal

From the envelope spectrum, it can be seen that the frequency component of this reconstructed signal is only the fault frequency component of the bearing, and its amplitude spectra after pre-whitening are the same. Fig. 11(b) is basically the same. There are some differences caused by the effect of noise. Therefore, the fault feature frequency can be extracted from the SGMD based on the quantitative law.

For comparison, the fault feature extraction method of the wavelet-SVD difference spectrum is introduced to

process the above signals. The obtained envelope spectrum is shown in Fig. 15. The feature frequency of the bearing outer fault can be seen from it, which is consistent with the feature frequency of the bearing outer fault extracted by this method. This further confirms the accuracy of the proposed method in extracting bearing fault features. However, the fault features of the inner were not extracted. Through comparison, it is found that the proposed method is more effective for extracting bearing fault features.

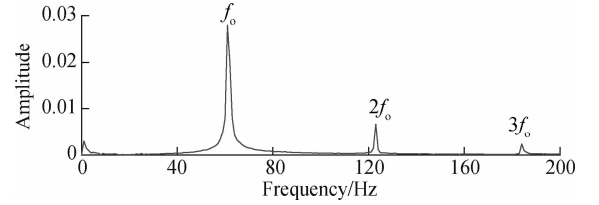


Fig. 15 Envelope spectrum of wavelet detail signal d3

6 Conclusions

1) This paper proposed a bearing fault diagnosis method based on CWP and SGMD's quantitative law. This method first processes the signal through CWP without determining the bearing resonance frequency band, and it can effectively eliminate the interference of background noise and discrete frequency components.

2) In this paper, we find that in the SGMD process, the number of α_i is twice that of the frequency components contained in the signal, and this number is applied to the feature extraction of bearing faults.

3) The initial symplectic geometric component can be effectively reconstructed by the quantitative law, and the feature frequency of the fault can be clearly extracted by Hilbert envelope spectrum analysis.

4) The performance of the proposed method is verified by the analysis of both simulated examples and an experimental signal. Furthermore, the method proposed in this paper is better than wavelet-SVD for extracting weak bearing fault features.

References

- [1] Zhao D, Liu S L, Gu D, et al. Improved multi-scale entropy and its application in rolling bearing fault feature extraction[J]. *Measurement*, 2020, **152**:107361. DOI: 10.1016/j.measurement.2019.107361.
- [2] Cui L L, Wang X, Xu Y G, et al. A novel switching unscented Kalman filter method for remaining useful life prediction of rolling bearing [J]. *Measurement*, 2019, **135**: 678 – 684. DOI:10.1016/j.measurement.2018.12.028.
- [3] Glowacz A, Glowacz W, Glowacz Z, et al. Early fault diagnosis of bearing and stator faults of the single-phase induction motor using acoustic signals[J]. *Measurement*, 2018, **113**: 1 – 9. DOI:10.1016/j.measurement.2017.08.036.
- [4] Su W S, Wang F T, Zhu H, et al. Rolling element bearing faults diagnosis based on optimal Morlet wavelet filter and autocorrelation enhancement [J]. *Mechanical Systems and Signal Processing*, 2010, **24**(5): 1458 – 1472. DOI:10.1016/j.ymssp.2009.11.011.

- [5] Liu J, Xu Z D, Zhou L, et al. A statistical feature investigation of the spalling propagation assessment for a ball bearing [J]. *Mechanism and Machine Theory*, 2019, **131**: 336 – 350. DOI:10.1016/j.mechmachtheory.2018.10.007.
- [6] Chen B J, Shen B M, Chen F F, et al. Fault diagnosis method based on integration of RSSD and wavelet transform to rolling bearing [J]. *Measurement*, 2019, **131**: 400 – 411. DOI:10.1016/j.measurement.2018.07.043.
- [7] Ding P, Jia M P, Wang H. A dynamic structure-adaptive symbolic approach for slewing bearings' life prediction under variable working conditions [J]. *Structural Health Monitoring*, 2020: 147592172092993. DOI: 10.1177/1475921720929939.
- [8] Jiang R L, Chen J, Dong G M, et al. The weak fault diagnosis and condition monitoring of rolling element bearing using minimum entropy deconvolution and envelop spectrum [J]. *Proceedings of the Institution of Mechanical Engineers, Part C: Journal of Mechanical Engineering Science*, 2013, **227**(5): 1116 – 1129. DOI: 10.1177/0954406212457892.
- [9] Sawalhi N, Randall R B. Signal pre-whitening using cepstrum editing (liftering) to enhance fault detection in rolling element bearings[C]// *Proceedings of the 24 International Congress on Condition Monitoring and Diagnostic Engineering Management*. Kolkata, India, 2011: 330 – 336.
- [10] Zhang X, Hu Y, Hu L, et al. Enhanced detection of bearing faults based on signal cepstrum pre-whitening and stochastic resonance[J]. *Journal of Mechanical Engineering*, 2012, **48**(23): 83 – 89. DOI:10.3901/JME.2012.23.083. (in Chinese)
- [11] Pan H Y, Yang Y, Li X, et al. Symplectic geometry mode decomposition and its application to rotating machinery compound fault diagnosis[J]. *Mechanical Systems and Signal Processing*, 2019, **114**: 189 – 211. DOI:10.1016/j.ymssp.2018.05.019.
- [12] Selesnick I W. Wavelet transform with tunable Q-factor [J]. *IEEE Transactions on Signal Processing*, 2011, **59**(8): 3560 – 3575. DOI:10.1109/tsp.2011.2143711.
- [13] Wu Z H, Huang N E. Ensemble empirical mode decomposition: A noise-assisted data analysis method[J]. *Advances in Adaptive Data Analysis*, 2009, **1**(1): 1 – 41. DOI:10.1142/s1793536909000047.
- [14] Cheng J. Local characteristic-scale decomposition method and its application to gear fault diagnosis[J]. *Journal of Mechanical Engineering*, 2012, **48**(09): 64 – 71. DOI: 10.3901/JME.2012.09.064. (in Chinese)
- [15] Yi C C, Lü Y, Dang Z, et al. Quaternion singular spectrum analysis using convex optimization and its application to fault diagnosis of rolling bearing[J]. *Measurement*, 2017, **103**: 321 – 332. DOI:10.1016/j.measurement.2017.02.047.
- [16] Yan X, Jia M, Morphological demodulation method based on improved singular spectrum decomposition and its application in rolling bearing fault diagnosis[J]. *Journal of Mechanical Engineering*, 2017, **53**(7): 104 – 112. DOI: 10.3901/JME.2017.07.104. (in Chinese)
- [17] Zhao X, Ye B, Chen T. Extraction method of faint fault feature based on wavelet-SVD difference spectrum[J]. *Journal of Mechanical Engineering*, 2012, **48**(7): 37 – 48. DOI:10.3901/JME.2012.07.037. (in Chinese)

基于倒谱预白化和辛几何模态分解数量规律的 轴承故障特征提取方法

陈奕雅¹ 贾民平¹ 鄢小安²

(¹东南大学机械工程学院, 南京 211189)

(²南京林业大学机械工程学院, 南京 210037)

摘要: 为了有效提取轴承的故障特征, 避免轴承损伤引起的冲击成分受到离散频率分量和背景噪声的干扰, 提出了一种基于倒谱编辑信号预白化和辛几何模态分解数量规律的轴承故障特征提取方法。首先, 对原始信号进行倒谱预白化来增强轴承故障的冲击特性, 去除复杂振动信号中的周期性频率成分, 产生只包含背景噪声和损伤引起的非平稳冲击成分的白化信号。其次, 发现了辛几何模态分解中哈密顿矩阵的有效特征值数目与信号中的频率个数成 2 倍的数量规律, 并通过仿真和理论推导验证了该数量规律。最后, 构造预白化信号的轨迹矩阵, 进行辛几何模态分解, 根据发现的数量规律, 选择相应的特征向量重构信号, 进行希尔伯特包络谱分析, 并提取故障特征。通过仿真分析和应用实例证明, 所提方法可以清晰地提取轴承的故障特征。

关键词: 倒谱预白化; 辛几何模态分解; 特征值; 数量规律; 特征提取

中图分类号: TH17